

Electrode-Dependent Electrical Properties of Detection-Band Tunable Ultraviolet Photodetectors Based on Ga₂O₃/GaN Heterostructures

Guanqi Li, Ruifan Tang, Na Gao,* Cheng Li, Jinchai Li, Kai Huang,* Junyong Kang, and Rong Zhang

The polycrystal Ga₂O₃ on GaN was realized by high-temperature oxidization of the GaN films with oxidation time 1 and 10 h, and the metal-semiconductor-metal photodetectors based on the Ga₂O₃/GaN heterostructure were fabricated by using Ti and Au metal electrodes. A comparative study of different electrodes and oxidation time on the performance of ultraviolet photodetector is performed. Among the devices prepared by 1 h oxidation, it is found that the device fabricated with Au electrode shows a lower dark-current and higher photocurrent than the one with Ti electrode. This is mainly due to the higher Schottky barrier height of sample with Au electrode. As for the device that experienced 10 h oxidation with Au electrode, the solar-blind responsivity with the full width at half maxima of 12 nm was obtained, which can be attributed to thicker Ga₂O₃ film. The devices exhibit excellent performance, including low dark-current and satisfactory responsivity, even under ultra-weak signal. The authors attribute these excellent properties to the Ga₂O₃ film, as it has a large grain size and a porous structure. The results provide a simple method that is low-cost and high-output with large-area production of high-performance ultraviolet photodetectors.

ZnMgO,^[5–7] LaAlO,^[8] etc.^[9] The alloying process is indispensable for the controllability of the detection wavelengths of solar-blind PDs. However, the manufacturing process is complex and leads to inevitably phases segregation, which will degrade the performance of solar-blind PDs.

The emergence of Ga₂O₃ semiconductors has shown unique advantages in avoiding the alloying process because of its ultrawide bandgap of 4.5–4.9 eV, covering the solar-blind regime and processing high thermal stability, chemical stability, and thermal conductivity.^[10–17] Also, a variety of thin-film growth methods have emerged in the past decades.^[18–27] Wu et al. have recently fabricated self-powered UVC PDs on the grown β-Ga₂O₃ film by laser molecular beam epitaxy (MBE) on ZnO substrate, which appears low dark current and a responsivity of 0.763 mA W⁻¹ without bias.^[28] Chen et al. have reported the β-Ga₂O₃ films on diamond substrates by

plasma-enhanced chemical vapor deposition (PECVD) with the device's faster response speed and the responsivity of 2.6 mA W⁻¹ at zero bias.^[11] Qian et al. have revealed that the PDs based on amorphous Ga₂O₃ films by magnetron sputtering had better performance than the β-Ga₂O₃.^[29] Guo et al. fabricated self-powered UV PDs through depositing an n-type Ga₂O₃ thin film onto an Al₂O₃ single-crystal substrate shielded by a p-type GaN thin film, and the device has a high UV/visible rejection ratio ($R_{254\text{ nm}}/R_{400\text{ nm}} = 5.9 \times 10^3$) under zero bias.^[30] However, these methods are high cost, low efficiency, and difficult for large-scale production.


Recently, the growth of Ga₂O₃ films by oxidization of GaN films at a high temperature is proposed as an effective method that is easy to control, low cost, and available for large-size production.^[31–34] A recent work by Weng et al. has reported the β-Ga₂O₃/GaN-based solar-blind and visible-blind dual-band PDs by furnace oxidization, achieving a deep-UV to a near-UV contrast ratio of 4.6×10^3 at a bias of 1 V.^[33] Tang et al. have implemented the surface-plasmon-enhanced PDs through depositing Rh nanoparticles onto the surface of the Ga₂O₃ by thermal oxidation, indicating the potentials in material preparation.^[34] On the other hand, the structures of the PDs play a key role in acquiring high-performance PDs. The lateral

1. Introduction

UV detection can be precisely divided into UVA, UVB, and UVC; the UVC detection, particularly, solar-blind photodetectors (PDs), has demonstrated great potential applications in flame detection, ozone hole monitoring, and secure communication. For most studies, the solar-blind PDs were fabricated based on wide-bandgap alloying semiconductors, such as AlGaIn,^[1–4]

G. Li, Dr. C. Li
School of Electronic Science and Engineering
Xiamen University
Xiamen 361005, P. R. China

G. Li, R. Tang, Dr. N. Gao, Prof. J. Li, Prof. K. Huang, Prof. J. Kang, Prof. R. Zhang
Collaborative Innovation Center for Optoelectronic Semiconductors and Efficient Devices
Department of Physics
Xiamen University
Xiamen 361005, P. R. China
E-mail: ngao@xmu.edu.cn; k_huang@xmu.edu.cn

 The ORCID identification number(s) for the author(s) of this article can be found under <https://doi.org/10.1002/pssa.202100166>.

DOI: 10.1002/pssa.202100166

metal–semiconductor–metal (MSM) structure is a widely used electrode pattern in PDs, and the metal–semiconductor is a critical matter to determine the carrier transport and then affect the device performance.^[35–39] Recently, Liu et al. have fabricated the β -Ga₂O₃-based ohmic- and Schottky-contacted detectors by comparing their optoelectrical behaviors and the fundamental physical mechanism between these two contacts.^[40] Guo et al. have grown the PDs based on β -Ga₂O₃ films by MBE, which presents good Schottky behaviors with lower dark current and faster rise time than ohmic detectors.^[41] In contrast, the Schottky contacts achieve better performances by engineering the Schottky barriers by different work functions between the metal electrode/semiconductor interface. Zhou et al. have utilized different electrodes on SrTiO₃ with the largest Schottky barrier height devices, enabling the lowest dark current and the highest responsivity.^[42] Li and Anderson have also pointed that the reduced dark current of the silicon-based MSM PDs could be attributed to higher Schottky barrier height due to the thermionic emission.^[43] However, the influence and inherent physical mechanism of different electrodes on the optoelectrical performance of Schottky-contacted PDs based on thermal oxide Ga₂O₃ films needs to be further studied.

In this work, the Ga₂O₃ films with different thicknesses were grown by thermally oxidizing GaN epitaxial films to form Ga₂O₃/GaN heterostructures. The MSM PDs were fabricated through controlled oxidation time and exhibited tunable response of broadband 250–370 nm and a solar-blind detection for oxidizing 1 and 10 h, respectively. By depositing Ti/Au and Au electrodes on the MSM PDs, the Schottky barrier height at the metal electrode/semiconductor interface is engineered, leading to the reduced dark current as low as 10⁻¹² A and a high detectivity of $\approx 1.28 \times 10^{14}$ Jones at 260 nm. This work provides a simple and effective pathway for the realizations of detection-band tunable UV PDs with low cost, large scale, and high performances.

2. Results and Discussion

Four samples of Ga₂O₃/GaN heterostructures were fabricated with the epitaxial GaN films thermally oxidized for 1 h (samples A and B) and 10 h (samples C and D), respectively. As shown from the top-view and cross-sectional images in **Figure 1a–c**, the surface morphologies of the GaN films have remarkably become rough after thermal oxidation, with the presence of large-size grains of Ga₂O₃ on the surface. Furthermore, there exhibit more grains, and the surface becomes rougher, as the oxidation time increases. From the SEM images, the thicknesses of Ga₂O₃ films in samples A and B are determined ≈ 500 to 700 nm, as described in our previous work.^[34] For samples C and D, the averaged thickness of Ga₂O₃ film corresponds to ≈ 3.7 to 3.9 μ m. Due to the transformation of GaN, the initial thickness of GaN is 5.1 to 5.2 μ m, and then achieves 4.8 to 4.9 μ m after oxidation for 1 h. However, the GaN layer thickness is ≈ 2.4 to 2.6 μ m after 10 h oxidation. Obviously, the oxidized GaN layer thickness is not varied linearly, as the thermal oxidation rate during growth at the surface, which significantly slows down the oxidation process between O₂ and GaN. The large-size grains on the surfaces are facilitated to improve the optical absorption by the increased surface-to-volume ratio. Meanwhile, the energy dispersive spectroscopy (EDS) analysis in **Figure 1d,e** represents the elemental N, O, and Ga distributions before and after oxidation, which indicates a large proportion of Ga and O elements and the switching from GaN to Ga₂O₃ structure. The appearance of aluminum may be caused by pollution in the oxidation furnace.

Based on the aforementioned Ga₂O₃/GaN heterostructures, a series of MSM PDs were fabricated by varying metal electrodes on different Ga₂O₃ thicknesses simultaneously. Four MSM PDs were prepared based on the grown Ga₂O₃/GaN heterostructures;

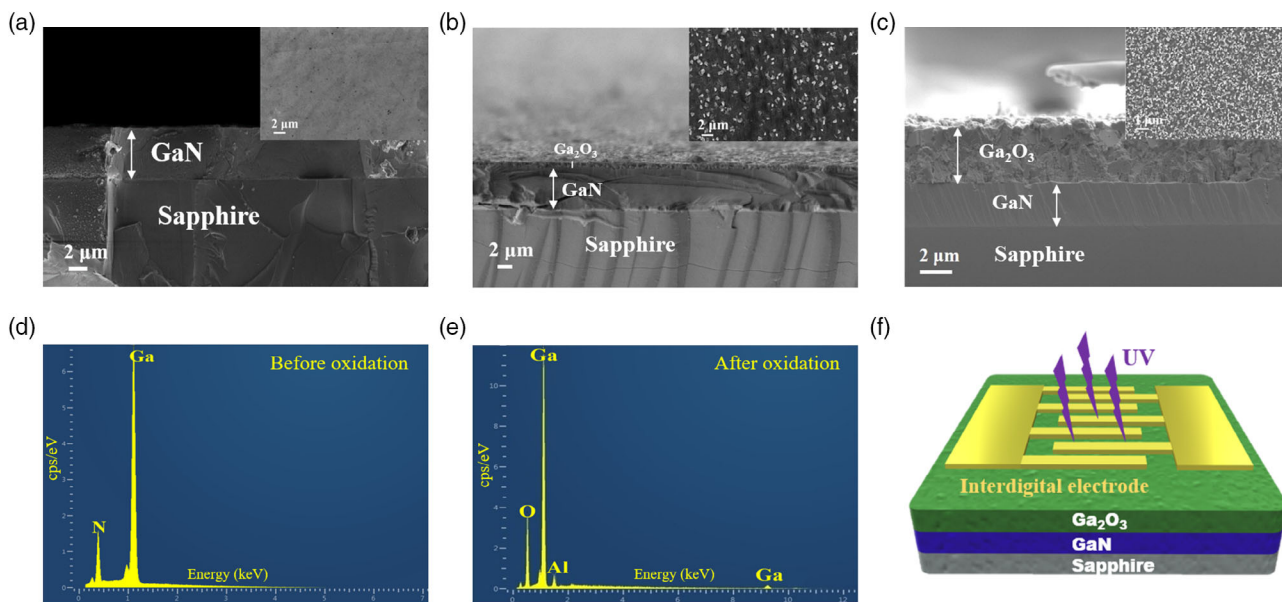


Figure 1. a–c) The cross-sectional and top-view (inset) FE-SEM images of the prepared Ga₂O₃/GaN heterostructures under 1 and 10 h oxidation time. d, e) The EDS spectrum before and after oxidation, respectively. f) Schematic diagram of the MSM-structured PD.

for samples A and B, the thicknesses of Ga₂O₃/GaN heterostructures are the same, but with different electrodes of Ti/Au (20/40 nm) and Au (40 nm), respectively. For samples C and D, the thickness of Ga₂O₃ is ≈3.7-3.9 μm for oxidizing at about 10 h, and the electrodes of Ti/Au (20/40 nm) and Au (40 nm) are also deposited. Figure 1f shows the 3D schematic of the designed structure of the representative device.

Figure 2 shows the *I*-*V* characteristics of the fabricated MSM PDs based on Ga₂O₃/GaN heterojunctions for samples A-D. Figure 2a shows the dark current and photocurrent under 260 nm illumination. Notably, the dark *I*-*V* curves and the *I*-*V* curves under illumination all exhibit Schottky features. The dark current is estimated to be as low as 10⁻¹² A under the low bias for four samples, indicating that our devices have low noise. When the bias increases to 15 V, the dark current of sample D is still as low as 10⁻¹² A, whereas that increases to 10⁻¹⁰ A for samples A and B and 10⁻¹¹ A for sample C. The low dark current in samples C and D can be attributed to the thicker Ga₂O₃ film, enabling the electrons channel to almost attenuate in the Ga₂O₃ layer rather than in the GaN layer. In contrast, the dark current of sample A increases faster with the increasing bias than sample B, which may attribute the lower Schottky barrier height determined by the work functions of

the Ti than the Au electrode. Moreover, samples C and D also exhibit the same behavior. Obviously, the Schottky barrier height formed by different electrodes has an effect on the dark current of the device.

Figure 2b shows the photocurrent of four samples under 360 nm illumination. Due to the depletion layer reaches the GaN with the increase of the bias, the photocurrent of samples A and B at 360 nm rises rapidly, so that the electrodes could collect the photogenerated carriers in the GaN, whereas the photocurrent of samples C and D at 360 nm only has a little rise due to the thicker Ga₂O₃ layer. In addition, two sets of samples exhibit almost the same photocurrent at 260 nm with a low bias of 0-2 V. As the bias increases, the depletion layer will reach to the GaN layer, resulting in a rapidly increased photocurrent due to the excellent conductivity of GaN for samples A and B.

To quantify the Schottky barrier height and the band structure of Ti electrode and Au electrode on Ga₂O₃, the in situ XPS was carried out to detect photoelectrons from a shallow surface depth, respectively.^[44-46] The position of the valence band maximum of Ga₂O₃ concerning the Fermi level (0 eV in the XPS spectra) can be directly measured. Figure 3a shows the valence band structure of the Ga₂O₃, and the cutoff was estimated at ≈3.51 eV separation from the Fermi level to valence band maximum.

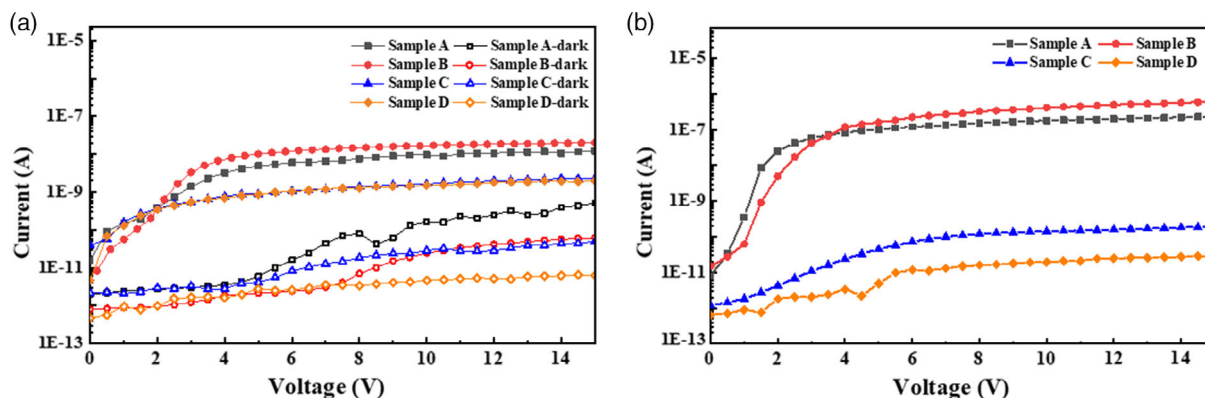


Figure 2. a) Illuminated and dark *I*-*V* characteristics of Ga₂O₃/GaN MSM UV PDs for samples A-D under 260 nm. b) Photocurrent of the four devices under 360 nm. The light intensities of 260 and 360 nm after calibration by the Si standard detector are 2.3 μWcm⁻² and 1 × 10⁻⁴ Wcm⁻².

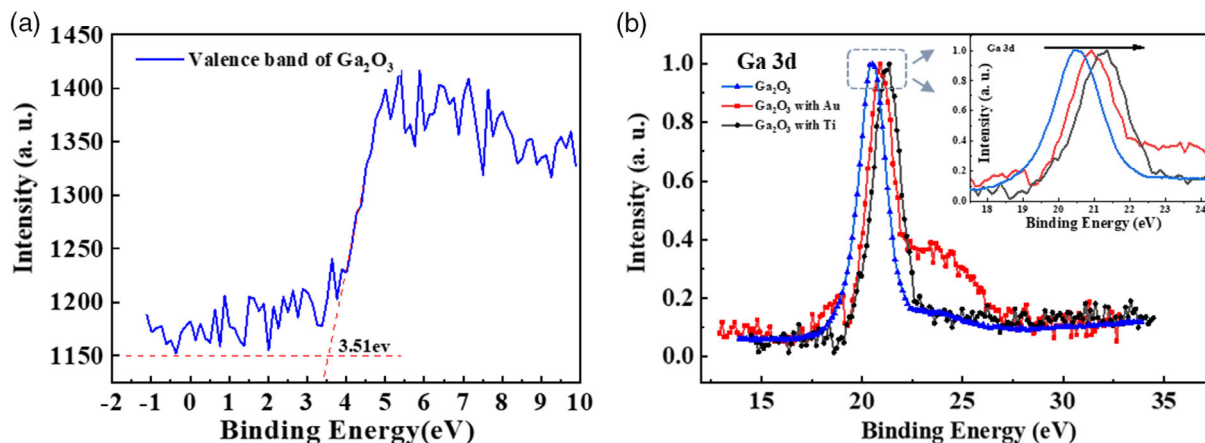


Figure 3. a) Valence band structure of Ga₂O₃. b) The core-level spectra of Ga 3d for Ga₂O₃ and Ga₂O₃ with Ti and Au.

The core-level spectra of Ga 3d for the initial Ga₂O₃ surface, Ti, and Au depositions are shown in Figure 3b. It clearly observes a red shift to the higher binding energies after the metal deposition. The Schottky barrier height is determined from the red shift to 0.4 and 0.85 eV for Ti electrode and Au electrode on Ga₂O₃, corresponding to all samples. Thus, the lower dark current of samples B and D aforementioned in Figure 2 can be explained by the higher Schottky barrier than the height of samples A and C. After the metal Au is deposited, the core level spectrum of Ga 3d for Ga₂O₃ with Au presents additional features. The features are located between 22.5 and 25 eV and are possibly related to the defect states of Ga or arising from the other compounds of Ga during the thermal process, or other defects formed during the Au deposition.

The key figures-of-merit responsivity (*R*) and detectivity (*D*^{*}) are used to evaluate the performance of the PDs. As shown in Figure 4a–d, samples A and B show a broad spectrum UV

response, whereas samples C and D exhibit a large 260 nm/360 nm rejection ratio exceeding 10³. It is worth noting that the responsivity spectrum of the MSM PDs is located at 250–370 nm for samples A and B, covering a broad range from UVC to UVA. The values of the responsivity are given by the following equation

$$R = \frac{I_{\text{ph}} - I_{\text{Dark}}}{P_{\text{optical}}} \quad (1)$$

where *I*_{ph} and *I*_{Dark} denote the photocurrent and the dark current, respectively, and *P*_{optical} is the incident optical power at the specific wavelength.

Obviously, the spectral responsivity reaches as high as 4.69 and 7.78 AW⁻¹ at a bias of 7 V for samples A and B, showing sharp cutoff drops by two orders of magnitude at ≈375 nm. As the dark current of sample D is lower, the responsivity of

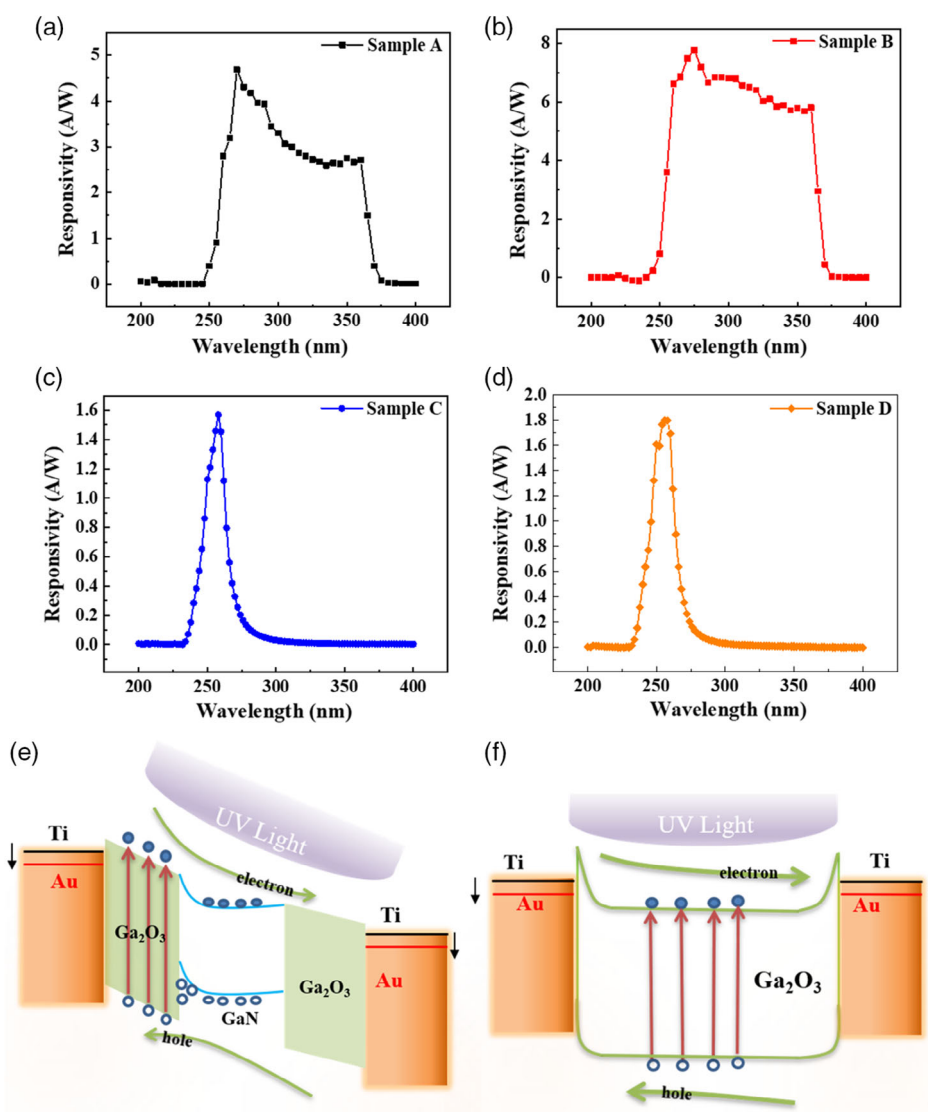


Figure 4. a-d) Spectral responsivity of Ga₂O₃ MSM UV PDs for all samples. All the devices are measured under 7 V. e,f) The energy band mechanism diagrams of samples with different electrodes and oxidation times.

sample D has also been enhanced. It can be seen that the Schottky barrier of the metal electrode/Ga₂O₃ interface has a significant influence on the performance of the device. When the height of the Schottky barrier is improved by ≈ 0.45 eV, the dark current decreases by one order of magnitude, and the responsivity of the device will be enhanced. Meanwhile, the spectral responses were tunable to a narrowband wavelength of 260 nm for samples C and D, with the full-width at half-maximum (FWHM) as narrow as 17 and 18 nm. The responsivity is determined as 1.57 and 1.8 AW⁻¹ at a bias of 7 V. Wang et al. has reported a solar-blind UV PD based on the poly(3,4-ethylenedioxythiophene) and polystyrene sulfonate acid (PEDOT:PSS)/ β -Ga₂O₃ structure, which shows a sharp cutoff wavelength at 263 nm with the FWHM as narrow as 17 nm.^[47] Liu et al. have fabricated the β -Ga₂O₃-based solar-blind PD, and the response spectrum also presents a narrowband behavior.^[48] In this work, the optical power density of the incident light is much lower compared with the reported work, particularly below the wavelength of 230 nm. Thus, in addition to the depletion layer attenuated to the Ga₂O₃ layer, the fewer photons absorption at the shorter wavelength is probably leading to the narrowband detection. The detectivity (D^*) could be expressed as

$$D^* = \frac{R}{\sqrt{2eI_{\text{Dark}}/S}} \quad (2)$$

where S (2.88×10^{-4} cm²) is the effective area under illumination. The shot noise from I_{Dark} is regarded as the major component in the total noise. The detectivity for sample A at a wavelength of 260 nm is calculated as 1.26×10^{13} Jones, which is of one order magnitude lower than sample B (1.28×10^{14} Jones).

Figure 4e,f represents the schematic band structures of the metal/semiconductor contacts. The formation of Au electrode on Ga₂O₃ (sample B) leads to a higher Schottky barrier than Ti metal on Ga₂O₃ (sample A), facilitated to suppress the dark current and improve the performances of the MSM PDs. Thus, the Au electrode is fabricated onto the surface of sample C that thermally oxidizing GaN films for 10 h. One can deduce from Figure 4f that the photogenerated carriers with relatively slow mobility in the Ga₂O₃ film enable only the UVC light absorbed by the Ga₂O₃ depletion layer, and the photocurrent exhibits lower than the other two PDs. Among the four PDs, sample B is expected to process the most stable performance, particularly showing a significant improvement in responsivity. Due to the lower dark current and higher photocurrent, the detectivity D^* for sample B at 260 nm is determined 1.28×10^{14} Jones at ≈ 260 nm, which is much larger than that of sample A (1.26×10^{13} Jones).

3. Conclusion

In this work, we obtain the polycrystal Ga₂O₃ by a simple process of high-temperature oxidization of GaN film with different oxidation times (1 and 10 h), and simple MSM structure PDs were fabricated. The PDs exhibited excellent performance, including low dark current ($\approx 10^{-12}$ A) and satisfactory responsivity (7.78 AW⁻¹) even under ultraweak signal (4.6×10^{-10} W).

Moreover, the devices fabricated by 1 h oxidation exhibit a broad spectrum UV response, and the sample with Au electrode has higher responsivity and lower dark current than the one with Ti electrode. When the bias exceeds 5 V, the dark current is far suppressed due to the formation of the higher Schottky barrier, which is consistent with the results obtained by XPS measurement. Due to lower dark current and higher photocurrent, the detectivity D^* for sample B at 260 nm is calculated as 1.28×10^{14} Jones, which is much larger than that of sample A (1.26×10^{13} Jones). The solar-blind responsivity with the FWHM of 18 nm was obtained when an oxidizing time of 10 h hour is performed. Due to the thickening of the Ga₂O₃ film, the photocurrent and the dark current are maintained at a low value compared with the devices prepared by 1 h oxidation. The good performance, along with the low-cost fabrication, and availability in solar-blind or broad-spectrum UV detection, indicates that our finding reveals additional pathways for developing UV PDs for various applications.

4. Experimental Section

The complete Ga₂O₃/GaN heterostructures were initiated with the n-type GaN film grown along with the *c*-plane sapphire substrates. Before the oxidation process, the GaN/sapphire was ultrasonically cleaned with acetone and alcohol in sequence and then immersed into a dilute aqueous hydrochloric acid solution (HCl:H₂O = 1:1) to remove the oxides on the surface. Subsequently, the samples were placed in a quartz tube furnace, with 50 standard-state cubic centimeter per minute (sccm) oxygen passed through at 1000 °C for 1 h and 10 h at atmospheric pressure, respectively. A series of characterizations were carried out to deeply understand the structural properties of the grown Ga₂O₃/GaN heterostructure. The surface morphology, crystalline quality, and element distribution of the samples were investigated by a Hitachi S-4800 field-emission scanning electron microscope (FE-SEM). The valence band and the electron binding energy were performed by an X-ray photoelectron spectroscopy (XPS; PHI Quantum 2000) using monochromatic Al K α X-rays.

Based on the grown Ga₂O₃/GaN heterostructures, a series of standard processes, such as photolithography (Karluss MA6/BA6), direct-current magnetron sputtering (Denton Explorer-14), and liftoff process, were carried out to fabricate MSM PDs. For the interdigitated MSM structures reported in this work, the fingers were 300 μ m long and 10 μ m wide with a spacing of 10 μ m. Ti/Au (20/40 nm) and Au (40 nm) were then sputtered to form Schottky contacts. The fabricated PDs were finally annealed by rapid thermal annealing (RTA 300) under a N₂ atmosphere at 400 °C for 300 s. *I*-*V* characteristics and the photocurrent response spectra were measured using a combination of a 450 W Xe arc lamp, Keithley 2410 source meter, and a Keithley 6514 programmable electrometer. The system was calibrated with a UV-enhanced Si detector. The devices were all illuminated from the front metal/semiconductor contact side, and the effective illumination area was $\approx 2.88 \times 10^{-4}$ cm². All measurements were carried out at room temperature.

Acknowledgements

The authors appreciate Shaoxiong Wu at Xiamen University for technical support for the device measurements. This work was supported by the National Key Research and Development Program (2016YFB0400903), the National Natural Science Foundation of China (61974126, 61874090, and 51902273), and the Natural Science Foundation of Fujian Province (2021H0001).

Conflict of Interest

The authors declare no conflict of interest.

Data Availability Statement

The datasets used or analysed during the current study are available from the corresponding author on reasonable request.

Keywords

Ga₂O₃, heterostructures, schottky barrier, ultraviolet photodetectors

Received: March 27, 2021

Revised: April 18, 2021

Published online: June 7, 2021

-
- [1] D. Walker, V. Kumar, K. Mi, P. Sandvik, P. Kung, X. H. Zhang, M. Razeghia, *Appl. Phys. Lett.* **2000**, *76*, 403.
- [2] Z. G. Shao, D. J. Chen, H. Lu, R. Zhang, D. P. Cao, W. J. Luo, Y. D. Zheng, L. Li, Z. H. Li, *IEEE Electron Device Lett.* **2014**, *35*, 372.
- [3] W. Zhang, J. Xu, W. Ye, Y. Li, Z. Qi, J. Dai, Z. Wu, C. Chen, J. Yin, J. Li, H. Jiang, Y. Fang, *Appl. Phys. Lett.* **2015**, *106*, 021112.
- [4] Y. Huang, D. J. Chen, H. Lu, K. X. Dong, R. Zhang, Y. D. Zheng, L. Li, Z. H. Li, *Appl. Phys. Lett.* **2012**, *101*, 253516.
- [5] M. M. Fan, K. W. Liu, X. Chen, X. Wang, Z. Z. Zhang, B. H. Li, D. Z. Shen, *ACS Appl. Mater. Interfaces* **2015**, *7*, 20600.
- [6] Y. Zhao, J. Zhang, D. Jiang, C. Shan, Z. Zhang, B. Yao, D. Zhao, D. Shen, A. C. S. *Appl. Mater. Interfaces* **2009**, *1*, 2428.
- [7] Y. M. Zhao, J. Y. Zhang, D. Y. Jiang, C. X. Shan, Z. Z. Zhang, B. Yao, D. X. Zhao, D. Z. Shen, A. C. S. *Appl. Mater. Interfaces* **2009**, *1*, 2428.
- [8] J. Xing, E. J. Guo, K. Jin, H. B. Lu, J. Wen, G. Z. Yang, *Opt. Lett.* **2009**, *34*, 1675.
- [9] L. Rigutti, M. Tchernycheva, A. De Luna Bugallo, G. Jacopin, F. H. Julien, L. F. Zagonel, K. March, O. Stephan, M. Kociak, R. Songmuang, *Nano Lett.* **2010**, *10*, 2939.
- [10] H. Chen, K. Liu, L. Hu, A. A. Al-Ghamdi, X. Fang, *Mater. Today* **2015**, *18*, 493.
- [11] Y. C. Chen, Y. J. Lu, C. N. Lin, Y. Z. Tian, C. J. Gao, L. Dong, C. X. Shan, *J. Mater. Chem. C* **2018**, *6*, 5727.
- [12] L. Li, E. Auer, M. Liao, X. Fang, T. Zhai, U. K. Gautam, A. Lugstein, Y. Koide, Y. Bando, D. Golberg, *Nanoscale* **2011**, *3*, 1120.
- [13] M. Razeghi, A. Rogalski, *J. Appl. Phys.* **1996**, *79*, 7433.
- [14] L. Sang, M. Liao, M. Sumiya, *Sensors* **2013**, *13*, 10482.
- [15] D. Y. Guo, H. Liu, P. Li, Z. P. Wu, S. L. Wang, C. Cui, C. R. Li, W. H. Tang, *ACS Appl. Mater. Interfaces* **2017**, *9*, 1619.
- [16] Y. B. Li, T. Tokizono, M. Y. Liao, M. Zhong, Y. Koide, I. Yamada, J. J. Delaunay, *Adv. Funct. Mater.* **2010**, *20*, 3972.
- [17] B. Zhao, F. Wang, H. Y. Chen, Y. P. Wang, M. M. Jiang, X. S. Fang, D. X. Zhao, *Nano Lett.* **2015**, *15*, 3988.
- [18] Y. Qin, H. D. Sun, S. B. Long, G. S. Tompa, T. Salagaj, H. Dong, Q. M. He, G. Z. Jian, Q. Liu, H. B. Lv, M. Liu, *IEEE Electron Device Lett.* **2019**, *40*, 1475.
- [19] F.-P. Yu, S.-L. Ou, D.-S. Wu, *Opt. Mater. Express* **2015**, *5*, 1240.
- [20] C.-Y. Huang, R.-H. Horng, D.-S. Wu, L.-W. Tu, H.-S. Kao, *Appl. Phys. Lett.* **2013**, *102*, 011119.
- [21] K. Arora, N. Goel, M. Kumar, M. Kumar, *ACS Photonics* **2018**, *5*, 2391.
- [22] S. Kang, U. Chatterjee, D. Y. Um, Y. T. Yu, I. S. Seo, C. R. Lee, *ACS Photonics* **2017**, *4*, 2595.
- [23] F. Boschi, M. Bosi, T. Berzina, E. Buffagni, C. Ferrari, R. Fornari, *J. Cryst. Growth* **2016**, *443*, 25.
- [24] D. Y. Guo, Z. P. Wu, P. G. Li, Y. H. An, H. Liu, X. C. Guo, H. Yan, G. F. Wang, C. L. Sun, L. H. Li, W. H. Tang, *Opt. Mater. Express* **2014**, *4*, 1067.
- [25] H. Lee, K. Kim, J.-J. Woo, D.-J. Jun, Y. Park, Y. Kim, H. W. Lee, Y. J. Cho, H. M. Cho, *Chem. Vap. Deposition* **2011**, *17*, 191.
- [26] D. Y. Guo, K. Chen, S. L. Wang, F. M. Wu, A. P. Liu, C. R. Li, P. G. Li, C. K. Tan, W. H. Tang, *Phys. Rev. Applied* **2020**, *13*, 024051.
- [27] C. Wu, D. Y. Guo, L. Y. Zhang, P. G. Li, F. B. Zhang, C. K. Tan, S. L. Wang, A. P. Liu, F. M. Wu, W. H. Tang, *Appl. Phys. Lett.* **2020**, *116*, 072102.
- [28] Z. P. Wu, L. Jiao, X. L. Wang, D. Y. Guo, W. H. Li, L. H. Li, F. Huang, W. H. Tang, *J. Mater. Chem. C* **2017**, *5*, 8688.
- [29] L. X. Qian, Z. H. Wu, Y. Y. Zhang, P. T. Lai, X. Z. Liu, Y. R. Li, *ACS Photonics* **2017**, *4*, 2203.
- [30] D. Y. Guo, Y. L. Su, H. Z. Shi, P. G. Li, N. Zhao, J. H. Ye, S. L. Wang, A. P. Liu, Z. W. Chen, C. R. Li, W. H. Tang, *ACS Nano* **2018**, *12*, 12827.
- [31] L. M. Lin, Y. Luo, P. T. Lai, K. M. Lau, *Thin Solid Films* **2006**, *515*, 2111.
- [32] W. Y. Weng, T. J. Hsueh, S. J. Chang, I. E. E. Senior Member, G. J. Huang, H. T. Hsueh, *IEEE Sensors Journal* **2011**, *11*, 1491.
- [33] W. Y. Weng, T. J. Hsueh, S. J. Chang, G. J. Huang, H. T. Hsueh, *IEEE Sensors Journal* **2011**, *11*, 999.
- [34] R. F. Tang, G. Q. Li, C. Li, J. C. Li, Y. F. Zhang, *Opt. Express* **2020**, *28*, 5731.
- [35] A. M. Cowley, S. M. Sze, *J. Appl. Phys.* **1965**, *36*, 3212.
- [36] W. Mnch, *Surf. Sci.* **1970**, *21*, 443.
- [37] R. T. Tung, *Phys. Rev. B* **1992**, *45*, 13509.
- [38] Y. Jiao, A. Hellman, Y. Fang, *Sci. Rep.* **2015**, *5*, 11374 .
- [39] J. G. Li, *Mater. Chem. Phys.* **1997**, *47*, 126.
- [40] Z. Liu, Y. S. Zhi, Y. Y. Liu, X. Tang, Z. Y. Yan, P. G. Li, X. H. Li, D. Y. Guo, Z. P. Wu, W. H. Tang, *J. Phys. D: Appl. Phys.* **2020**, *53*, 085105.
- [41] D. Y. Guo, Z. P. Wu, Y. H. An, X. C. Guo, X. L. Chu, C. L. Sun, L. H. Li, P. G. Li, W. H. Tang, *Appl. Phys. Lett.* **2014**, *105*, 023507.
- [42] W. J. Zhou, K. J. Jin, H. Z. Guo, C. Ge, M. He, H.-B. Lu, *Journal of Applied Physics* **2013**, *114*, 224503.
- [43] M. Y. Li, W. A. Anderson, *Solid-State Electronics* **2007**, *51*, 94.
- [44] W. E. Spicer, I. Lindau, P. Skeath, C. Y. Su, P. Chye, *Phys. Rev. Lett.* **1980**, *44*, 420.
- [45] L. Diederich, *Surf. Sci.* **1998**, *418*, 219.
- [46] N. Fujimura, A. Ohta, K. Makihara, S. Miyazaki, *Jpn. J. Appl. Phys.* **2016**, *55*, 08PC06.
- [47] H. B. Wang, H. Y. Chen, L. Li, Y. F. Wang, L. X. Su, W. P. Bian, B. S. Li, X. S. Fang, *J. Phys. Chem. Lett.* **2019**, *10*, 6850.
- [48] Z. Liu, X. Wang, Y. Y. Liu, D. Y. Guo, S. Li, Z. Y. Yan, C.-K. Tan, W. J. Li, P. G. Li, W. H. Tang, *J. Mater. Chem. C* **2019**, *7*, 13920.